

# Electromagnetic Shielding Characteristics of Optical-Fiber Feedthroughs

Keith D. Masterson, *Member, IEEE*, David R. Novotny, and Galen H. Koepke

**Abstract**—A number of commercially available optical-fiber connector styles ST, SC, and FC were tested to determine the extent to which their use in bulkhead adapter feedthroughs would compromise the shielding of electromagnetic interference for electronic enclosures. Connectors and adapter barrels made from metal, ceramic, and polymer materials were included in the tests. The tests were carried out using a nested reverberation cell and covered a frequency range from 1 to 16 GHz. Although we rely on data acquired by making shielding effectiveness (SE) measurements, we report the results in terms of a transmission cross section which is the ratio of the power coupled into an enclosure through an aperture to the power per unit area incident on the aperture. The amount of coupling through the feedthroughs we tested varied over 70 dB. The shielding of an all-metal FC connector system was nearly equal to that of a blank reference plate. In some cases, a feedthrough coupled more energy into the enclosure than was coupled through the empty hole required to mount the adapter barrel. Unlike SE, the transmission cross sections do not depend on the volume, shape, or construction materials of the enclosure and can be used to estimate the degradation in the SE for enclosures other than our reference cell. The uncertainties in the reported transmission cross sections are calculated to be  $\pm 3$  dB and are small compared to the differences between the measured cross sections.

**Index Terms**—Electromagnetic interference, fiber optic adapter barrels, fiber optic connectors, fiber optics, shielding effectiveness, mode-stirred chamber.

## I. INTRODUCTION

WE HAVE tested a number of commercially available optical-fiber, adapter-barrel feedthroughs to determine the extent that they would compromise the shielding of electronic enclosures against electromagnetic interference (EMI) [1]. In this paper, we report the measurement techniques, data analysis, and uncertainty analysis together with the results. The result are expected to be of considerable interest to engineers involved in designing optical-fiber links for electromagnetic environments, to provide base line data for possible additional studies, and to aid the development of standard procedures to evaluate the shielding effectiveness (SE) of a variety of optoelectronic components.

Although optical-fiber is immune to EMI, photodiodes, laser diodes, and their associated electronic circuitry are not. These components must be placed in shielded enclosures with filtered supplies in order to operate satisfactorily in an environment

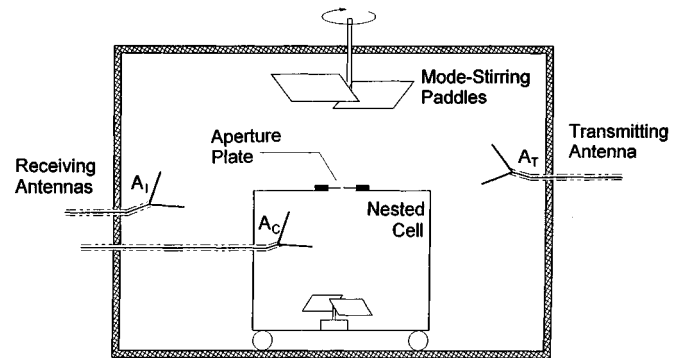


Fig. 1. Configuration of reverberation chamber and nested cell for SE measurements.

of strong EMI. Therefore, leakage of electromagnetic energy around optical-fiber feedthroughs and into shielded enclosures is a significant problem, and one which we expect to worsen as bandwidth and data rates increase. This is especially true for analog links used in demanding metrology applications such as often are encountered at the National Institute of Standards and Technology (NIST). Although fiber feedthroughs that provide excellent shielding for critical applications can be custom made, in many cases it is expedient to use commercially available adapter-barrel feedthroughs. The degree to which the SE of an enclosure is compromised by those feedthroughs having polymer bodies is of special interest.

## II. THEORY

The SE of an enclosure is very dependent on its geometry and construction materials. Therefore, we compare the SE of a reference enclosure with the feedthrough installed to the SE of that same enclosure with a small reference aperture and then calculate a transmission cross section for the feedthrough. The transmission cross section can then be used to estimate the degradation in the SE of more practical enclosures that use the same feedthrough system. We closely follow the work of Hill *et al.* [2] who studied the aperture excitation of large cavities. The experimental arrangement consists of nested, mode-stirred reverberation cells as shown in Fig. 1. The inner cell is our reference enclosure. The cells operate much like common microwave ovens. Power radiated by the transmitting antenna  $A_T$  establishes an RF field between the cells. The mode-stirring paddles assure that all modes are excited and the resultant fields are isotropic when averaged over time. Because of high RF reflectance and low losses at the cell walls, relatively high electrical fields can be established around the nested cell with modest input power

Manuscript received July 14, 1997; revised December 6, 2000. This work was supported by the National Institute of Standards and Technology Advanced Technology Program Office.

The authors are with the Electromagnetic Fields Division, National Institute of Standards and Technology, Boulder, CO 80305 USA.

Publisher Item Identifier S 0018-9375(01)04066-2.

to the transmitting antenna ( $> 00$  V/m with inputs of  $< 10$  W). Also, only a slight leakage into the reference cell results in a measurable signal from the receiving antenna  $A_C$ .

The SE of an enclosure is defined from the ratio of the power density  $S_I$  incident on the enclosure and monitored with the receiving antenna  $A_I$  to the power density  $S_C$  inside the enclosure and monitored with the receiving antenna  $A_C$  as

$$SE = 10 \log_{10} \left| \frac{S_I}{S_C} \right|. \quad (1)$$

For an enclosure with a small aperture and containing no source, SE is always positive. The ratio  $S_I/S_C$  is given formally by [2] as

$$\frac{S_I}{S_C} = \frac{2kV}{\langle \sigma_T \rangle} \frac{1}{Q} = \frac{2kV}{\langle \sigma_T \rangle} \sum \frac{1}{Q_i} \quad (2)$$

where

- $k$  wavenumber of the incident EM radiation;
- $\langle \sigma_T \rangle$  transmission cross section of the aperture averaged for uniform, isotropic incident radiation of wavelength  $2\pi/k$ ;
- $V$  volume of the enclosure;
- $Q$  quality factor for the electrical characteristics of the enclosure;
- $Q_i$  contribution of a particular loss mechanism to the total  $Q$  of the enclosure.

The values of  $S_I/S_C$  and  $V$  can be determined directly by experimental measurements. If we also know the  $Q$  of the enclosure, we can obtain the transmission cross section for the feedthrough. However, an accurate determination of the  $Q$  is difficult by either direct experimental measurements or theoretical calculations. Fortunately, we can avoid having to explicitly determine the cavity  $Q$  by measuring the SE of the enclosure with an installed feedthrough relative to the SE of the same enclosure with a well defined reference aperture and then determine the transmission cross section of the feedthrough in relation to that of the reference aperture.

Nevertheless, it is instructive to estimate and compare the various losses from the enclosure. Using the expressions in [2] together with the geometry and materials of our nested cell, we have calculated  $Q_1$  due to the absorption in the enclosure walls,  $Q_2$  due to the power coupled into the receiving antenna, and  $Q_3$  due to the power radiated back out of a small open aperture. For the conductivity of the walls, we used the value of  $8.83 \times 10^6$  S/m that was experimentally measured for an aluminum alloy similar to that from which our nested cell was fabricated [2]. The results are shown in Fig. 2. At frequencies below 1 GHz, the absorption by the receiving antenna is dominant. Above this frequency, the dominant loss is absorption by the enclosure walls. The loss back out the small aperture is insignificant at low frequencies and is more than 20 dB below the wall loss at high frequencies.

Additional power can be absorbed by cable jackets, connectors, and various metal components that are inside the enclosure and are necessary for the measurement system to work. Since these materials are poor absorbers, we expect this contribution to be relatively small. We add  $Q_4$  to account for these losses and

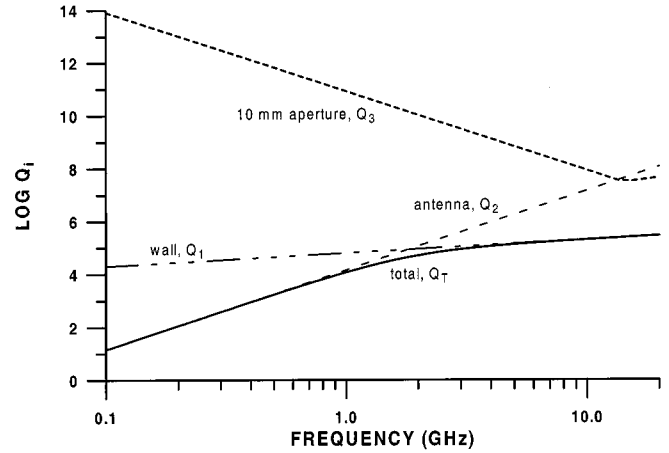


Fig. 2.  $Q$  of the nested cell and contributions due to various loss mechanisms.

leave it to be determined as a small correction term that provides the fit between the theoretically predicted SE for a small circular reference aperture and the experimentally measured data.

The power transmitted through an open aperture is given in [2] as

$$\frac{1}{Q_3} = \frac{\langle \sigma_T \rangle}{2Vk}. \quad (3)$$

Although an exact theoretical solution for the transmission coefficient of a circular aperture in a thin conducting sheet is available in terms of spheroidal functions [3] and solutions based on variational approximations have been reported by Levine and Schwinger [4] for normal incidence, we used the approximate solutions for electrically small and electrically large apertures of radius  $a$  given by Hill *et al.* [2] as

$$\langle \sigma_T \rangle_S = \frac{16}{9\pi} k^4 a^6, \quad \text{electrically small} \quad (4)$$

and

$$\langle \sigma_T \rangle_L = \frac{\pi a^2}{2}, \quad \text{electrically large} \quad (5)$$

Fig. 3 shows the approximation for normal incidence together with those for electrically small and electrically large cases. Since the experimental data from [2] also indicate a resonance in the transmission cross section near  $ka = 1.5$ , we chose  $\langle \sigma_T \rangle = \langle \sigma_T \rangle_S$  up to  $ka = 1.4$  and then linearly connect this with  $\langle \sigma_T \rangle = \langle \sigma_T \rangle_L$  for  $ka \geq 5$  as shown. These relations define the reference values for the open apertures that we used to determine the transmission cross sections of the feedthroughs. Using (3) together with the assumption that the transmission cross sections for electromagnetic energy entering and leaving the test enclosure through the open aperture are the same, we can express (2) as

$$\frac{S_I}{S_C} = \frac{2Vk}{\langle \sigma_T \rangle} \left[ \frac{1}{Q_P} \right] + 1 \quad (6)$$

where

$$\frac{1}{Q_P} = \frac{1}{Q} - \frac{1}{Q_3} \quad (7)$$

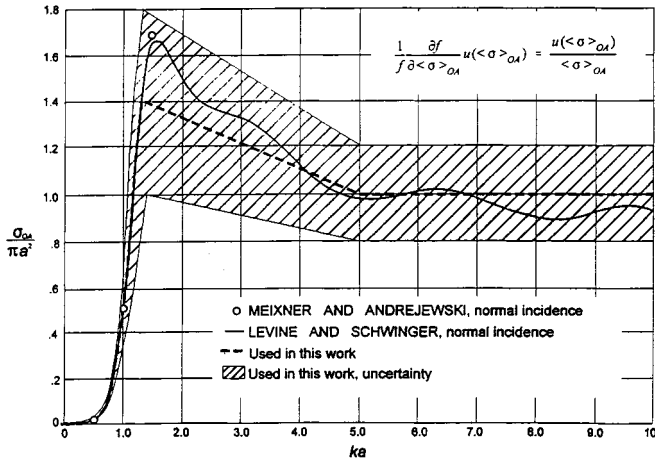


Fig. 3. Transmission cross section and uncertainty for a circular aperture. The values are normalized to the electrically large limit given by (5).

and  $Q_P$  includes all the losses except for the transmission back out through the aperture or feedthrough. If a feedthrough is partially absorbing, the energy lost from inside the enclosure will be slightly larger than the transmission of energy into the enclosure. However, by lowering the feedthrough into the cell during the SE measurements for the reference aperture, the absorption due to it is included in  $Q_P$ . The feedthroughs we tested were very small compared to the size of the nested cell and constructed of metals and dielectrics which have little absorption. The very small difference in the absorption of the feedthrough between having it inside the cell or mounted in the cell wall is considerably less than our measurement uncertainty, and  $Q_P$  is indistinguishable from a constant during a measurement sequence used for a particular adapter barrel. Thus, the measured transmission cross section for a feedthrough can be expressed in terms of the theoretical values for the small open apertures as

$$\frac{\langle \sigma_T \rangle_{FT}}{\langle \sigma_T \rangle_{OA}} = \frac{(S_I/S_C)_{OA} - 1}{(S_I/S_C)_{FT} - 1}. \quad (8)$$

The ratio  $S_I/S_C$  is obtained from the spectrum analyzers used to accumulate the data as

$$\frac{S_I}{S_C} = \frac{F_{ISA} F_{IC} F_{IAF}}{F_{CSA} F_{CC} F_{CAF}} \cdot \frac{SN_I}{SN_C} = \frac{R}{F} \quad (9)$$

where

- $F_{ISA}$  calibration factor for the spectrum analyzer I;
- $F_{IC}$  calibration factor for losses in cables to spectrum analyzer I;
- $F_{IAF}$  transfer function for antenna I;
- $F$  combined transfer coefficient that is independent of the feedthrough under test;
- $SN_I$  numerical output from a spectrum analyzer I;
- $R = SN_I/SN_C$ .

### III. EXPERIMENTAL PROCEDURE

#### A. Test and Connector Matrix

We performed measurements on three readily available optical-fiber connector systems that represent the most cost-effective approach for optical-fiber links in many applications. Although the origin of the nomenclature is obscure, the three

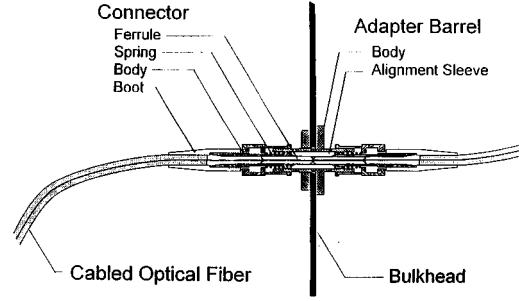


Fig. 4. Detail of a typical optical-fiber, bulkhead feedthrough.

styles are designated as ST, SC, and FC/PC by the industry. These styles all have similar basic construction utilizing connector bodies, precision ferrules to secure the fibers, and sleeves in adaptor barrels to properly align the ferrules. The various components are identified in the cross section of a typical feedthrough shown in Fig. 4. The ST and FC styles are available in a variety of material combinations ranging from all dielectric to all metal, and include metal connector and adapter bodies with either stainless steel or ceramic ferrules and alignment sleeves. This provided an opportunity to separately study a number of variables that might affect the SE of a feedthrough. The SC system is primarily of polymer and ceramic construction. However, we used SC adapter barrels with both metal and ceramic alignment sleeves. Limited resources did not permit us to test all the combinations. Instead, we tested representative all-metal and all-dielectric systems and then a mix of some of the metal and dielectric components in order to get an idea of the performance of systems that might occur in general use. Table I lists the various connectors and adapter barrels that we tested together with their construction materials. For brevity and convenience throughout the rest of the paper, we assign the codes given in column 3 to the various test configurations. For example, STMP is an all-metal ST connector mated with a polymer adapter barrel having a ceramic alignment sleeve. SCD refers to the duplex style SC connector, which holds two fibers and consists of side-by-side SC connectors.

#### B. Apparatus

The large reverberation chamber and its use in general EMI/EMC studies is described in detail by Crawford and Koepke [5]. Table II summarizes the basic characteristics of it and the nested cell.

The nested cell has a square port (225 mm on each side) to which a test plate can be mounted. Fig. 5 shows a cross section of a plate in the mounting frame with the double row of finger-stock seals to minimize unwanted leakage of electromagnetic energy. To further suppress leakage into the cell, we also placed a 30-mm wide strip of steel wool between the plate and the mounting frame as shown. We mounted the adapter barrels in a 300-mm square, 1.6-mm thick aluminum test plate following the manufactures' recommended procedures. No effort was made to increase the shielding by adding extra gaskets under the feedthroughs. However, before assembly all contact surfaces on the plate and cell wall were buffed with steel wool to remove any oxide layers.

TABLE I  
CONNECTORS, COMPONENTS, AND MATERIALS USED IN TEST MATRIX

SET	TYPE	CODE*	CONNECTOR		ADAPTER BARREL	
			Body	Ferrule	Body	Alignment sleeve
1	ST	STMM	metal	stainless	metal	stainless
2	ST	STMP	metal	stainless	polymer	ceramic
3	ST	STPP	polymer	ceramic	polymer	ceramic
4	ST	STOA	9.5 mm dia. open aperture			
5	FC	FCMM	metal	stainless	metal	stainless
6	FC	FCMC	metal	ceramic	metal	stainless
7	FC	FCMP	polymer	ceramic	metal	stainless
8	FC	FCOA	9.0 mm dia. open aperture			
9	SC	SCPP	polymer	ceramic	polymer	ceramic
10	SC	SCPM	polymer	ceramic	polymer	metal
11	SC	SCOA	9.9 mm by 13.6 mm open aperture			
12	SC-DUP	SCDP	polymer	ceramic	polymer	ceramic
13	SC-DUP	SCDO	9.9 mm by 26.4 mm open aperture			
14	SC-DUP	SCDT	As in 12 but with long dimension bisected with 2 mm wide conducting strip			
15	REF	REF	Blank reference plate with no aperture			
16	Open Port	LGOA	0.25 m by 0.25 m open, mounting port			

\* For convenience, we assign a code such as STMP to the ST connector with a metal body and ferrule coupled with a polymer adapter barrel having a ceramic alignment sleeve.

TABLE II  
CHARACTERISTICS OF THE REVERBERATION CHAMBER AND THE NESTED CELL

	Material	Dimensions (m)			Low Frequency	Approx. Q
		Length	Width	Height	Cutoff	
Large reverberation chamber	Painted Steel	4.57	3.05	2.74	~500 MHZ	~10 <sup>5</sup>
Access door	"		1.23	2.13		
Stir paddles	Al alloy	~1.42	~0.71		irregular	
Nested cell	Welded Al alloy	1.48	1.16	1.43	~1 GHz	~10 <sup>5</sup>
Access door	Al alloy		0.63	0.78		
Stir paddles	"	0.61	0.46		rectangle	

To obtain high EMI immunity for the signal lines between the nested cell and the bulkhead into the large reverberation chamber, we used semi-rigid coaxial cable. The dc line to the mode-stirring paddle in the nested cell was shielded and filtered. All electrical connections were wrapped in steel wool and then covered with electrically conducting tape.

### C. Data Acquisition

Data were acquired for each feedthrough configuration using the instrumentation shown in Fig. 6 and described in [1]. The broadband, open horn receiving antennas were a matched pair with frequency responses from 800 MHz to 16 GHz. Since appropriate power amplifiers only cover about one octave in fre-

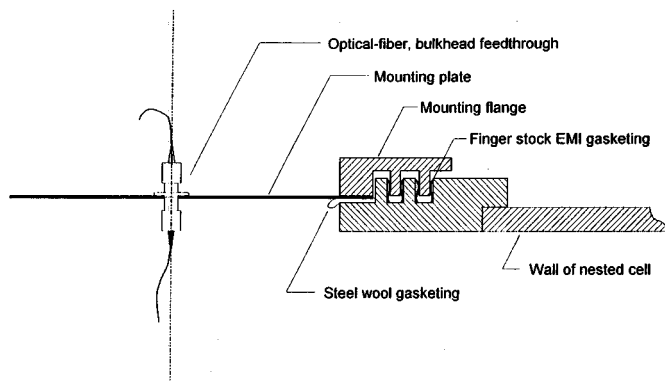


Fig. 5. Detail for securing the mounting plate to the nested cell.

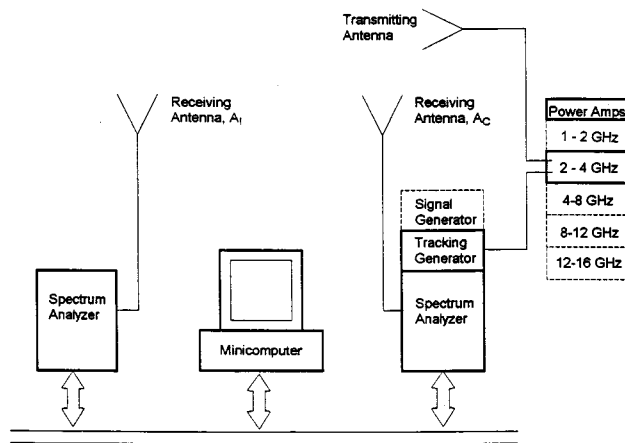


Fig. 6. Instrumentation for data acquisition.

quency, we had to continually switch between six different amplifiers in order to cover the 1–16-GHz range and maintain between 3–10 W of input power.

We first measured a solid, blank reference plate to determine the leakage into the nested cell and to establish a maximum SE that could be detected above the noise. Then we mounted a plate with an installed optical-fiber feedthrough and measured the SE. Finally, without disturbing the mounting plate, we removed the external connector, detached the adapter barrel, lowered it into the nested cell, and repeated the SE measurement. The total time to acquire data over the 1–16-GHz frequency range was about 10 h/connector configuration.

At frequencies above 2.7 GHz, we used a mode-stirred technique where the input is repetitively swept across a frequency band, while the metal stirring paddles are slowly rotated to mix the cavity modes and establish a field that is nearly isotropic when averaged over time. The weak signal from the receiving antenna inside the nested cell was accumulated by a spectrum analyzer with a tracking generator that supplied the input to the power amplifiers. We could not synchronize the second spectrum analyzer with the tracking generator, so the stronger signal from the antenna between the chamber walls was accumulated by a free-running spectrum analyzer.

At frequencies below the 2.7-GHz cutoff of our tracking generator, we left the signal generator at a set frequency while the spectrum analyzers accumulated data over many paddle wheel revolutions. This generally results in more accurate data at the

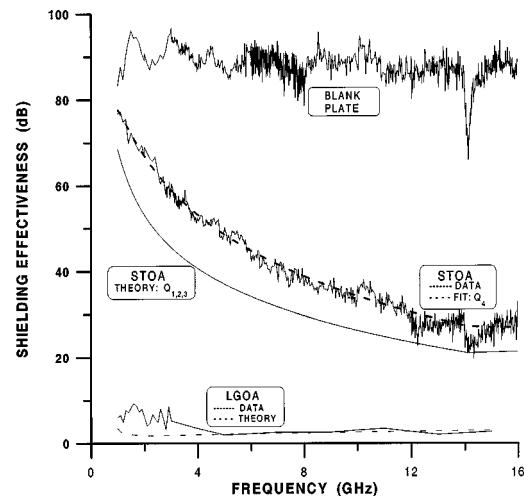


Fig. 7. Baseline values for the SE of the nested cell.

measurement frequency, but allows the possibility of missing narrow resonances that would show up in swept frequency measurements. However, we do not expect any narrow resonances at the lower frequencies for the connector systems under study because their physical dimensions are much smaller than a wavelength of the electromagnetic field.

We accumulated data in a peak-hold mode on each spectrum analyzer and averaged long enough to ensure that mode and channel filling were complete. Although theoretical values for the transmission cross section are modeled more accurately by an averaged signal, the approximate 8-dB increase in the signal obtained using the peak-hold method cancels when the ratio of the two signals is taken.

#### IV. DATA ANALYSIS

Our goal is to calculate the transmission cross sections for the bulkhead feedthroughs using (8) and the SE data. We applied the transfer coefficient to the 7000 points between 2.7 and 16 GHz, that were accumulated for each feedthrough system to obtain the ratios  $S_I/S_C$  as a function of frequency. The experimental data from reverberation chamber measurements are typically very noisy because of the statistical mixing of the many possible modes. Therefore, we applied a smoothing procedure which reduced each data set to about 700 points. The procedure consisted of replacing the value of each data point with the value obtained for it from a second-order least-squares fit to the nine points centered on it. Then, each third point of the set was saved into a reduced data set. Each spectral trace was smoothed twice using this algorithm. Fig. 7 shows the resulting traces for the blank reference plate and a plate with the 9.5-mm diameter open aperture required to mount the ST bulkhead adapter. The data from 6 to 8 GHz for the blank reference plate are shown before smoothing. There is no significant loss in sharp spectral features for the smoothed curves. The curve for the blank plate shows a sharp dip at 14 GHz, which we attribute to a resonance in the leakage through one of the door seals in the enclosure. At the bottom of the figure we have also included limited data acquired for the SE of the open, large square mounting port (0.25 m by 0.25 m).

TABLE III  
FITTING PARAMETERS FOR OPEN APERTURES

Aperture	Parameter		
	A	B	C
ST	$-(2.83 \pm 3.68) 10^{-4}$	$1.357 \pm 0.064$	$-22.6 \pm 1.9$
FC	$-(2.8 \pm 1.3) 10^{-3}$	$2.75 \pm 0.14$	$-45.8 \pm 2.8$
SC	$(1.81 \pm 0.08) 10^{-3}$	$1.013 \pm 0.047$	$-9.63 \pm 1.35$

The SE we calculate from theory for a 9.5-mm diameter aperture in our reference enclosure is the smooth, featureless solid curve labeled STOA in Fig. 7. However, the raw data show occasional step-like jumps that always occur at frequencies where we physically changed the input and output cables to the power amplifiers. Their cause was later traced to a bad cable connector. We used the theoretical curves and other experimental evidence to correct the spectral traces for most cases where short segments of the data were clearly out of line with the rest of the curve.

A smooth, continuous analytical expression which fits both the theory of small, open apertures and the experimentally obtained values for  $(S_I/S_C)_{OA}$  is desirable in order to remove the statistical fluctuations from the data and allow interpolation to any desired frequency within the experimental limits. The theoretical curve for STOA lies about 7 dB below the experimental data. This implies the presence of additional losses such as higher than expected wall losses or absorption by other materials in the cell which lower the  $Q$ . Especially significant was an observation that some steel wool was likely left exposed at the lip of the mounting plate as shown in Fig. 5. We estimated the additional absorption by an aperture equal to the surface area of the exposed steel wool and applied (5) across all  $ka$ , since the currents that would normally flow around the boundary of an electrically small aperture would be attenuated in the steel wool. When we added a term  $Q_4$  to (2) to account for this loss, the recalculated SE gave a much better fit to the observed data. In order to obtain an analytical expression for  $(S_I/S_C)_{OA}$  that more accurately fit the experimental data and includes other losses in the enclosure, we let

$$\frac{1}{Q_4} = \frac{A}{k^1} + \frac{B}{k^2} + \frac{C}{k^3} \quad (10)$$

and used a standard regression analysis [6] to determine the fitting parameters  $A$ ,  $B$ , and  $C$ . The resulting fit matches the experimental data well, as shown by the dashed line. The fitting parameters calculated for the apertures used with the ST, SC, and FC connectors are given in Table III. Variations in the fitting parameters arise from different amounts of steel wool left exposed, the effects of the faulty coaxial connector, and inaccuracies in the simple theory for describing the transmission of the reference apertures.

We calculated the transmission cross sections for the various feedthroughs using (8), the theoretical values for the reference apertures, the experimental data for  $(S_I/S_C)_{FT}$ , and the curves fit to the data for  $(S_I/S_C)_{OA}$ . The results are presented in graphical form in Figs. 8–10. The smooth, solid curves in the

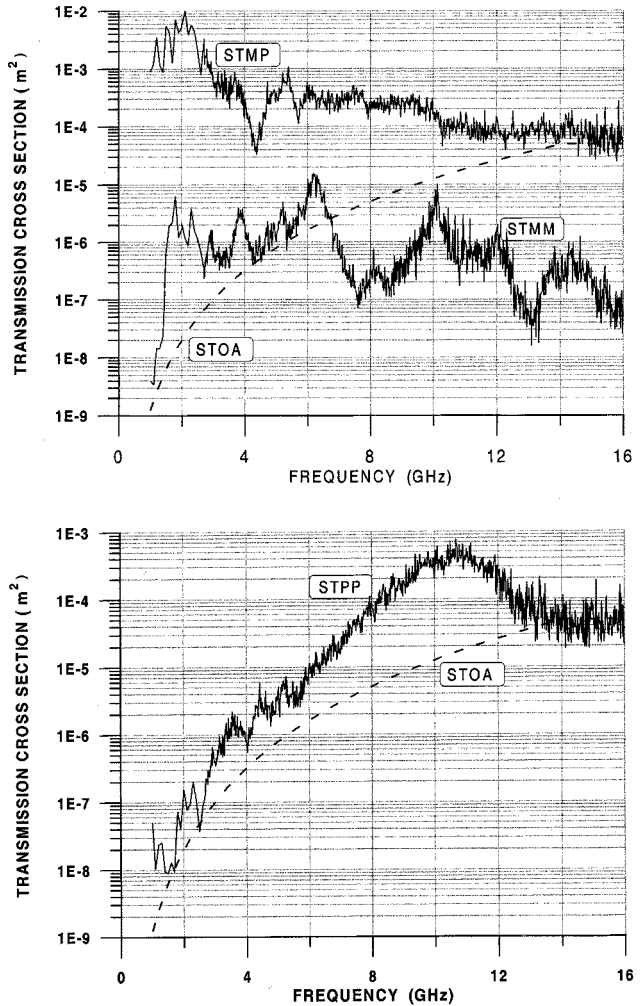


Fig. 8. Transmission Cross Sections for ST optical-fiber feedthroughs. The connector components associated with the label codes are given in Table I.

figures are the fits to  $(S_I/S_C)_{OA}$  that we obtained by using the fitting parameters shown in Table III for  $Q_4$ . The dashed curve is the fit to the 9.5-mm open aperture and is included as a common reference in all the plots.

## V. UNCERTAINTY ANALYSIS

We use (8) as the starting point for a standard propagation of uncertainties [7] for the measured transmission cross sections. We differentiate (8) by parts, normalize by the total cross section, conclude that the various component uncertainties are independent and uncorrelated, and finally sum the squares of the

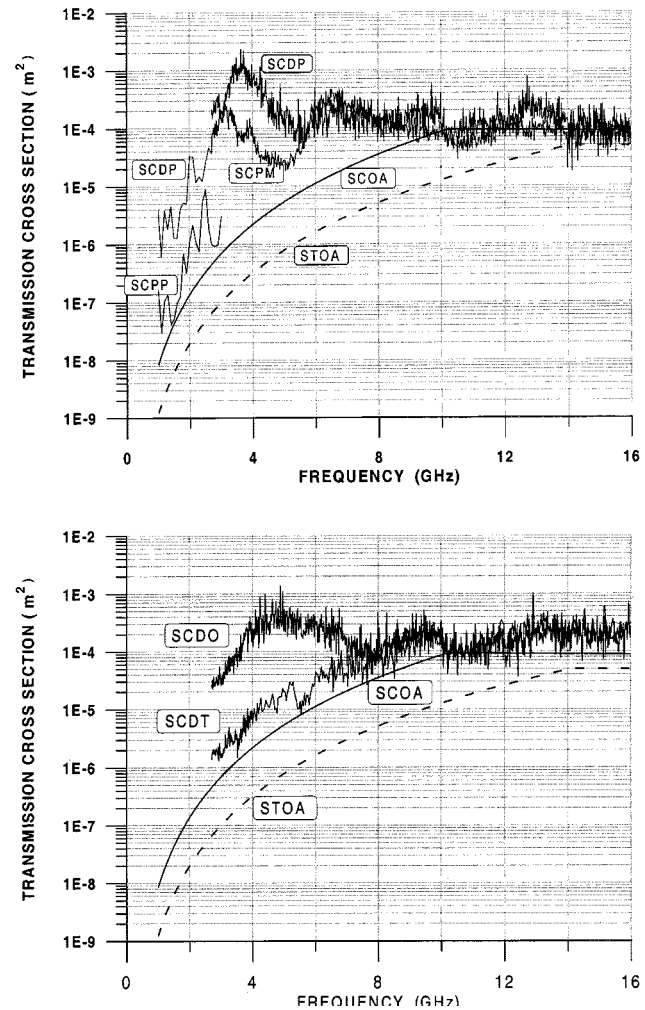


Fig. 10. Transmission Cross Sections for SC optical-fiber feedthroughs. The connector components associated with the label codes are given in Table I.

trically large and electrically small approximations, especially in the transition region. Previous studies [2] have shown these approximations to give good agreement with data for circular apertures at the high and low frequency ends of the spectrum. In the transition region where  $1 < ka < 10$ , minor resonances appear to be present. They are consistent with cross sections approximated from theory by Levine and Schwinger [4] for normal incidence. Accurate data for all angles of incidence are not available in the literature. We chose a rectangular distribution with the error bounds shown in Fig. 3 for the uncertainty in  $\langle \sigma_T \rangle_{QA}$ .

Our experimental data for the rectangular aperture of the single-fiber, simplex system (SCOA) were fit well with a circular aperture of equivalent area. However, for the higher aspect ratio aperture of the duplex style feedthrough (SCDO) this worked well only for the electrically large approximation. Numerical analysis of rectangular apertures [8] indicates that for  $ka \ll 1$  the transmission cross section for the SC-duplex aperture would be only about 1 dB over that of a circle with equal area. The larger deviation that we observe is probably due to resonances that are more important near  $ka = 1$ . When we placed a 1-mm wide piece of conducting copper-foil tape across the center of the aperture, the measured SE was nearly that expected for two of the SC-simplex apertures. Therefore, we

concluded that  $Q_P$  was close enough to that for the SC-simplex aperture that we could also use the SCOA data as the reference for the SC-duplex measurements. We think that the increase in the uncertainty for the transmission cross section measured for the SC-duplex feedthrough due to this choice of a reference is considerably less than the uncertainties in the values for the reference aperture itself, or to the statistical errors associated with  $(S_I/S_C)_{FT}$ .

### B. Uncertainties in the Ratios for $S_I/S_C$

We use the curves fitted to the  $(S_I/S_C)_{OA}$  data to determine the transmission cross sections. The uncertainties for the fitting parameters were calculated from the covariance matrices provided by a standard regression analysis. Although the residuals between the experimental data and the fitted curves show a small somewhat periodic dependence that appears to be reproduced in three of the four data sets, we can find no explanation for this in the physics of the measurement and conclude the effect is an artifact of the instrumentation. Since the errors associated with  $(S_I/S_C)_{OA}$  are much smaller than the total uncertainty, there is no compelling reason to pursue a better fit.

We use the root-mean-square of the residuals between the fitted curves and the experimental data for the open apertures as the basic uncertainty in the values for  $(S_I/S_C)_{FT}$ . The normalized uncertainty was uniform across frequency and SE. This is a conservative approach since it includes regions where the data for the open aperture are not centered about the fitted curve. Because of the occasional correction in the data to compensate for the effect of the faulty coaxial connector, we estimate the uncertainty in  $(S_I/S_C)_{FT}^2$  to be two times larger than the mean square of the residuals. Since this effect is intermittent in the data, we have included it as a random uncertainty rather than as a systematic error in the calibration factor for the cable.

### C. Uncertainties in the Calibration Factors

The uncertainties in the individual calibration factors are determined by manufacturers' specifications and NIST calibration data. We calibrated the spectrum analyzers frequently during the experiment using known input signals and obtained the calibration uncertainties give in Table IV. They are about 1 dB below the manufacturer's specifications. The two receiving antennas are a closely matched pair, so  $F_{IAF}/F_{CAF} \approx 1$ , and systematic errors in their calibrated response should cancel. However, we applied the uncertainty quoted by the manufacturer to each antenna factor separately. The calibration of the coaxial cables on a network analyzer provides an uncertainty of about 0.5 dB. The contribution to the total error from systematic errors in the calibration factors is small. Furthermore, almost all values of  $S_I/S_C$  are greater than 100 so that any systematic error in these ratios due to the transfer constant nearly cancels from the numerator and denominator of (8).

### D. Combined Standard Uncertainty

The root-mean-square combined fractional uncertainty for the transmission cross section is shown in Fig. 11. It was obtained by adding the component fractional uncertainties according to (11). The primary contribution is the large uncer-

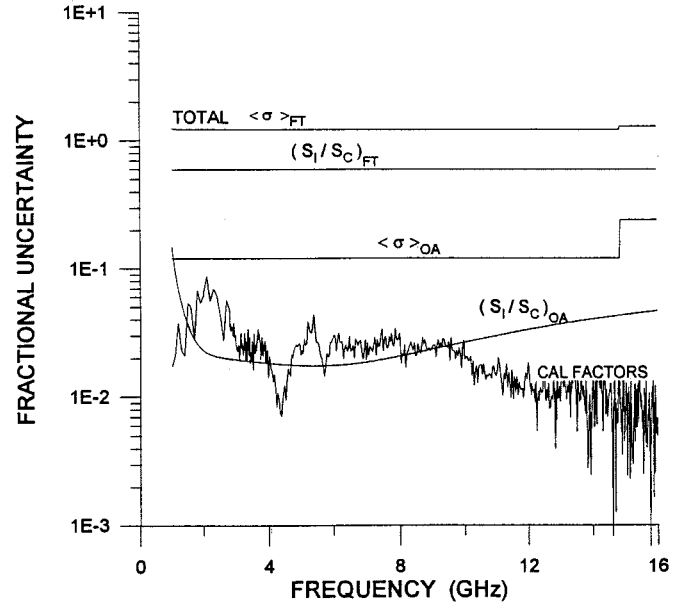


Fig. 11. Fractional uncertainties for measured transmission cross sections. The result for  $\langle \sigma_T \rangle_{FT}$  is for a coverage factor of 2 corresponding to a 95% confidence interval.

tainty associated with  $(S_I/S_C)_{FT}$ . The next most significant contribution is for the theoretical values used for the transmission cross section of the small circular apertures. An uncertainty of  $\pm 3$  dB is typical for measurements using reverberation cells.

## VI. CONCLUSIONS

We have successfully measured the ability of several optical-fiber bulkhead feedthrough systems to maintain the SE of a reference enclosure. The transmission cross sections calculated for the various feedthroughs range over eight orders of magnitude with uncertainties of  $\pm 3$  dB. The results are all considerably above the noise limits of the measurement system. The results also clearly show the superiority of the FC metal/metal adapter for maintaining the integrity of a shielded enclosure.

Several of the feedthrough combinations degraded the shielding beyond that of the open aperture required for their installation. In the STMP system, the metal connectors through the center of the dielectric adapter barrel form a dipole in the aperture that increases the coupling of electromagnetic radiation into the enclosure. Most polymer connectors (such as those used in STPP, SCPP, and SCDT) have small metal springs between the outer shell and the ferrule. Together with dielectric materials which can act as flux concentrators, the small springs can also increase the coupling of radiation into the enclosure. In the case of the SC simplex connector system, an adapter barrel with a ceramic alignment sleeve was used for the low frequency measurement (SCPP), but the adapter used for the high frequency measurement (SCPM) had a metal alignment sleeve. A substantial increase in the transmission cross section is evident at 2.7 GHz where we changed the adapter barrel.

The curves labeled SCDT and SCDO in Fig. 10 are for the transmission cross sections of the SC-duplex style connectors, with and without a 1-mm wide piece of conducting tape across the center of the aperture. The conducting strip reduces the transmission cross section at low frequencies ( $ka < 1$ ) to



TABLE IV  
FRACTIONAL COMPONENT UNCERTAINTIES FOR THE TRANSMISSION CROSS SECTIONS

Source	Spectral dependence	Type	Maximum uncertainty rectangular distribution dB	Standard Uncertainty dB
Reference cross section	Yes	B	1.5 $1 < ka < 4$ 0.8 otherwise	0.9 0.5
Signal ratio for reference aperture	calculated using covariance matrix			0.3
Fitting parameter A	Yes	A		3
Fitting parameter B	Yes	A		0.2
Fitting parameter C	Yes	A		0.6
Signal ratio for feedthrough	Yes	A		2
Calibration factor, F				0.3
Spectrum analyzer	No	B	0.5	0.3
Antenna transfer function	Yes	B	0.05	0.03
Cable loss *	Yes	B	0.1	0.05

\* This uncertainty does not include effects due to the faulty connector that we have added into the uncertainty in the signal ratios for the feedthroughs.

about twice that for a SC-simplex feedthrough. For applications that require SC-duplex connectors, we recommend the use of a conducting strip. This would require either an adapter barrel that would accommodate the strip or two single adapter barrels mounted with dimensions to match the duplex connectors.

The SE of practical electronic enclosures with optical-fiber feedthroughs can be estimated by using the transmission cross sections that we have reported. However, the leakage of energy into an enclosure is also dependent on its particular geometry and orientation with respect to the incident electromagnetic fields.

We have demonstrated a basic measurement technique that can be used to test the SE of a variety of connectors. The basic techniques can be applied to other types of devices and could be adapted for testing active components such as connector-mounted laser diodes and photodiodes. Data acquisition could be speeded up by using two spectrum analyzers that could be locked to a single tracking generator. Both acquisition time and signal-to-noise ratio could be improved through the use of a network analyzer to accumulate data. Finally, better theoretical calculations and numerical analysis for the coupling of isotropic radiation through a small circular aperture would reduce the uncertainties in the reference cross sections.

#### ACKNOWLEDGMENT

The authors wish to thank J. Ladbury and D. Camell for considerable help in setting up the experimental equipment and data acquisition system, D. Hill for the helpful discussions throughout the project, D. Vecchia for valuable help in statistical and uncertainty analysis, and D. Kuchta and J. Crow of IBM for their suggestion to place the narrow strip of conducting tape across the aperture for the duplex SC adapter barrel in order to increase the shielding.

#### REFERENCES

- [1] *Electromagnetic shielding characteristics of optical-fiber connectors*, Natl. Inst. Stand. Technol. Note 1383, 1997.
- [2] D. A. Hill, M. T. Ma, A. R. Ondrejka, B. J. Riddle, M. L. Crawford, and R. T. Johnk, "Aperture excitation of electrically large, lossy cavities," *IEEE Trans. Electromagn. Compat.*, vol. 36, pp. 169–177, Aug. 1994.
- [3] J. Meixner and W. Andrejewski, "Strenge theorie der beugung ebener elektromagnetischer wellen an der vollkommen leitenden kreisscheibe und an der kreisformigen offnung im vollkommen leitenden ebenen schirm," *Annal. Phys.*, vol. 7, no. 3/4, pp. 157–168, 1950.
- [4] H. Levine and J. Schwinger, "On the theory of electromagnetic wave diffraction by an aperture in an infinite plane conducting screen," *Comm. Pure Appl. Math.*, vol. 3, no. 4, pp. 355–391, 1950.
- [5] *Design, evaluation, and use of a reverberation chamber for performing electromagnetic susceptibility/vulnerability measurements*, Nat. Bur. Stand. (US) Tech. Note 1092, 1986.
- [6] D. W. Marquardt, "An algorithm for least squares estimation of non-linear parameters," *J. Soc. Ind. Appl. Math.*, vol. 11, no. 2, pp. 431–441, 1963.
- [7] *Guidelines for evaluating and expressing the uncertainty of NIST measurement results*, Natl. Inst. Stand. Technol. Tech. Note 1297, 1994.
- [8] F. de Meulenaere and J. Van Bladel, "Polarizability of some small apertures," *IEEE Trans. Antennas Propagat.*, vol. AP-25, pp. 198–205, Mar. 1977.

**Keith D. Masterson** (M'00) received the B.A. degree from Oregon State University, Corvallis, OR, in 1963 and the Ph.D. degree in physics from the University of Arizona, Tucson, AZ, in 1974, where his graduate work was in the area of atomic spectroscopy and optical sciences.

During 1966–1967 he worked in the area of laser-microprobe spectroscopy at the Institute for Spectrochemistry and Applied Spectroscopy, Dortmund, Germany. From 1974 to 1984 he worked on optical materials for solar energy conversion, first at the University of Arizona and later as a Senior Scientist at the Solar Energy Research Institute, Golden, CO. Since 1984, he has been at the National Standards of Technology's RF Technology Division, Boulder, CO, as project leader to develop optically sensed probes for measuring electromagnetic fields.

Dr. Masterson is a member of the Optical Society of America, SPIE-The International Society of Optical Engineering.

**David R. Novotny** was born in Minneapolis, MN in 1968. He received the B.S. and M.S. degrees from the University of Colorado, Boulder, in 1990 and 1996. His graduate work focused on designing specialized, nonperturbing dielectric mounts for antennas.

He is currently working at the National Institute of Standards and Technology, Boulder, CO, in the RF Technology Division, where he is working on new probes for EM field metrology and field generation techniques for antenna calibration purposes.

**Galen Koepke** received the B.S. degree in electrical engineering from the University of Nebraska, Lincoln, in 1973 and the M.S.E. E. degree from the University of Colorado, Boulder, in 1981.

He held research and teaching assistantships with the University of Colorado, spent several years working in forestry with the U.S.D.A. and was active in other areas of agriculture. In 1980, he joined the staff of the Radio Frequency Technology Division at the National Institute of Standards and Technology (NIST), where his responsibilities have included research in electromagnetic interference measurements and facilities, instrumentation, field probe, and antenna development, antenna calibrations and measurements; and software development for measurement processes.